Tin-Catalyzed Plasma-Assisted Growth of Silicon Nanowires

ARTICLE *in* THE JOURNAL OF PHYSICAL CHEMISTRY C · FEBRUARY 2011

Impact Factor: 4.77 · DOI: 10.1021/jp1066428

10 AUTHORS, INCLUDING:

Somilkumar J. Rathi
Intel, Hillsboro Or, USA
11 PUBLICATIONS **92** CITATIONS
SEE PROFILE

Bhavin Jariwala
Lam Research Corporation
13 PUBLICATIONS **94** CITATIONS
SEE PROFILE

THE JOURNAL OF PHYSICAL CHEMISTRY C

ARTICLE

pubs.acs.org/JPCC

Tin-Catalyzed Plasma-Assisted Growth of Silicon Nanowires

Somilkumar J. Rathi,[†] Bhavin N. Jariwala,[‡] Joseph D. Beach,[†] Paul Stradins,[§] P. Craig Taylor,[†] Xiaojun Weng,[∥] Yue Ke,[∥] Joan M. Redwing,[∥] Sumit Agarwal,[‡] and Reuben T. Collins*[,†]

[†]Department of Physics, Renewable Energy Materials Research Science and Engineering Center, Colorado School of Mines, Golden, Colorado 80401, United States

[‡]Department of Chemical Engineering, Renewable Energy Materials Research Science and Engineering Center, Colorado School of Mines, Golden, Colorado 80401, United States

[§]National Renewable Energy Laboratory, Golden, Colorado 80401, United States

[∥]Materials Research Institute, Department of Materials Science and Engineering, The Pennsylvania State University, University Park, Pennsylvania 16802, United States

Supporting Information

ABSTRACT: A systematic study of tin-catalyzed vapor−liquid−solid (VLS) growth of silicon nanowires by plasma-enhanced chemical vapor deposition at temperatures ranging from 300 to 400 °C is presented. Wire structure, morphology, and growth rate are characterized as a function of process variables. The nanowires are observed to have a crystalline core with a polycrystalline shell due to simultaneous VLS axial growth and vapor−solid radial growth. Axial and radial growth rates are controllable through hydrogen dilution of the plasma which affects the concentration of silane radicals in the plasma. In addition, wire length is observed to saturate with increasing growth time. Post growth chemical analysis suggests this is due to etching and disappearance of tin seeds in the hydrogen plasma which occur in parallel with wire growth. This opens up the possibility of a unique in situ approach to fabricating metal-free nanowire arrays for device applications.

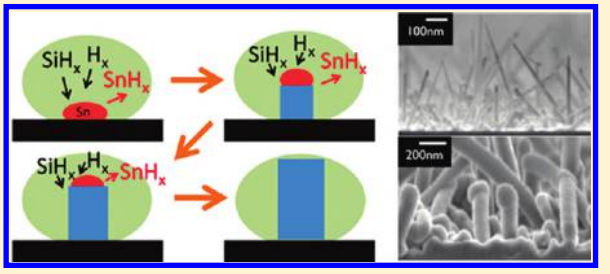

1. INTRODUCTION

Over the past decade, semiconducting nanostructures have attracted much attention due to their potential applications as building blocks in novel nanoscale devices. Specifically, silicon nanowires (SiNWs),[1] with their unique unidimensional structure with radial confinement,[2] potential for high material quality,[3] enhanced light-trapping properties,[4,5] and compatibility with existing silicon processing technology,[6,7] are promising candidates for more efficient photovoltaic devices.[8] To date, a variety of growth techniques have been developed[1,9−11] to synthesize high-quality SiNWs, but vapor−liquid−solid (VLS)-based chemical vapor deposition (CVD) remains the most common and extensively explored method. In general, semiconducting wire formation requires growth in one direction to occur much more rapidly than in others. In VLS-based, CVD growth, this is accomplished through use of a metal seed which catalyzes decomposition of a gas-phase silicon precursor. When the concentration of silicon in the seed exceeds saturation, a solid silicon phase forms and grows at the interface between the seed and the metal resulting in formation of a wire.

Several issues exist with thermal CVD-based VLS synthesis of SiNWs for photovoltaic applications. To achieve desirable growth rates, substrate temperatures of 500 °C or higher are typically required which limits the choice of substrates. In addition, agglomeration and coarsening of the metal seeds or vaporization of the catalyst can also occur at elevated temperatures.[12] The effect of the metal seed on wire properties is also an important consideration.[13] Au has historically been the most common metal catalyst.[14] Au is known, however, to adversely affect the minority carrier lifetime in bulk silicon.[15,16] Seeds like Au with high silicon and/or dopant solubility tend to have long residence times for growth elements, making it difficult to create abrupt junctions in the axial direction.[17] In addition, the metal seed needs to be removed during device fabrication to avoid shorting or contamination.

Sn is an interesting alternative Si nanowire catalyst. As a column IV element, Sn is isoelectronic with Si and hence a neutral impurity. It has been reported to form vacancy complexes in bulk Si but only after introducing damage through, for example, electron irradiation.[18] Compared to metals such as Ni and Pt, Sn does not form any intermediate compounds such as silicides.[19,20] Sn also has extremely low silicon solubility.[21] The Si−Sn eutectic point (and Sn melting point) is 232 °C,[22] a value much lower than that of Au (363 °C) and potentially ideal for low-temperature growth. To take

Received: July 16, 2010
Revised: November 23, 2010
Published: February 18, 2011

advantage of the low melting point, however, requires a growth process in which the precursor gas decomposition can be catalyzed by the seed at such low temperatures. Plasma-enhanced chemical vapor deposition (PECVD) in combination with Sn seeds opens up this possibility. By dissociating the precursor gas in a low power plasma, PECVD allows the substrate temperature to be lowered while maintaining high nanowire growth rates.[23−26]

While much research effort has been directed toward understanding the growth of SiNWs using Au, and alternative catalysts have recently received increased attention, only a very few preliminary studies have been reported for Sn-catalyzed SiNWs. Chi et al.[27] fabricated SnO_2-capped SiNWs using high-temperature CVD with an oxide-assisted growth mechanism. Yu et al.[28,29] synthesized Si wires on SnO_2-coated substrates by forming seeds using a hydrogen plasma, described the growth kinetics of Sn-catalyzed SiNWs, and proposed a model to account for the formation of a core−shell structure and significant sidewall faceting. Jeon and co-workers[30] demonstrated the growth of Sn-seeded SiNWs by hydrogen radical assisted deposition from SiH_4. Parlevliet et al.[31] demonstrated ribbon-like nanowires from pulsed PECVD growth using Sn seeds.

This article reports a systematic study of the low-temperature growth of silicon nanowires by PECVD using Sn as an alternative metal seed. Wire structure, morphology, and growth rate are characterized as a function of process conditions. Postgrowth chemical analysis indicates, surprisingly, that the ends of the wires are catalyst-free. An explanation for this along with an understanding of the effect of H_2 dilution on growth rates is presented. By comprehensively exploring the fundamental issues associated with Sn-seeded VLS growth, this work provides an important foundation for the use of Sn-seeded nanowires in device applications.

2. EXPERIMENTAL SECTION

The SiNWs were synthesized in a PECVD cluster tool. The reactor consists of a stainless steel vacuum chamber with a base pressure of $\sim 10^{-7}$ Torr. The capacitively coupled plasma was generated between the radio frequency (rf) powered and the grounded electrodes. For all of the studies presented here, the electrode spacing was set at 1.5 cm with an rf power of 20 W (plasma power density 195 mW/cm^2) at 13.56 MHz applied to the powered electrode via a matching network. The substrate was placed on the grounded electrode and heated to temperatures from 280 to 400 °C. To prepare substrates for growth, Si(111) *n*-type wafers were degreased with acetone and methanol followed by a 30 min UV ozone treatment. The surface oxide was removed in a buffered oxide etchant solution (6 parts 40% NH_4F and 1 part 49% HF) for 2 min and dried under N_2 flow. A 1-nm-thick Sn film was thermally evaporated at a base pressure of 10^{-6} Torr onto the polished side of the substrate at room temperature. Sn nanoseeds were formed by annealing the substrate in the deposition chamber at a temperature of 400 °C under vacuum for 2 h and subsequently exposing it to a H_2 plasma for 2 min with an H_2 flow rate of 36 sccm (std. cm^3/min at STP) at 1.4 Torr pressure while maintaining a 400 °C substrate temperature. The plasma treatment was included to reduce any oxide on the Sn surface and was done prior to the introduction of the SiH_4 gas. Wires were then grown on the substrate without breaking the vacuum. The SiH_4 flow rate was kept constant at 4 sccm for all of the studies reported, while the H_2 flow rate was varied from 36 to 100 sccm. This resulted in SiH_4 partial pressures that varied from 0.05 to 0.14 Torr, while the corresponding H_2 partial pressures varied from 1.35 to 1.26 Torr. The deposition duration was over the range of 2−40 min at a total chamber pressure of 1.4 Torr. Imaging, morphological, and elemental analyses of wires were performed using a field emission scanning electron microscope (JEOL JSM 7000F) and a scanning transmission electron microscope (JEOL 2010F) operated at 200 keV. X-ray energy dispersive spectrometry (XEDS) under STEM mode, high-resolution TEM, and selected area diffraction (SAD) were employed to determine the structure and chemical composition of the nanowires. Individual element scans used passed energy at 20 eV. Optical emission spectroscopy (OES) studies of the plasma were performed through a glass viewport mounted on the chamber wall. The emitted light was collected via a split fiber assembly and analyzed with an SD 200 Ocean Optics Inc. spectrometer. Emission lines for SiH* ($A^2\Delta \rightarrow X^2\Pi$; λ = 414 nm)[32] and Ar* ($4p'[1/2] \rightarrow 4s'[1/2]^0$; λ = 750 nm)[32] were recorded.

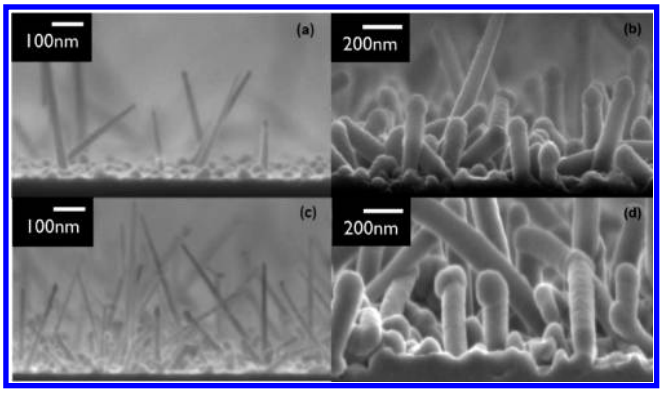

Figure 1. (a)−(d) SEMs showing variation in the diameter and length of the SiNWs as a function of the growth duration and H_2 dilution at a constant substrate temperature of 400 °C. For (a) and (c) the growth duration was 2 min with an H_2 flow of 100 sccm (1.35 Torr partial pressure) and 36 sccm (1.26 Torr partial pressure), respectively. For (b) and (d) the growth duration was 20 min with an H_2 flow of 100 sccm (1.35 Torr partial pressure) and 36 sccm (1.26 Torr partial pressure), respectively.

3. RESULTS AND DISCUSSION

SiNWs were grown in a SiH_4/H_2 plasma on Sn seeded Si(111) substrates. No SiNW growth was observed without the Sn catalyst or H_2 dilution of SiH_4. Wire growth was observed for temperatures from 280 to 400 °C, although the growth rate dropped substantially at lower temperatures. Figure 1(a)−(d) shows cross-sectional SEM images of SiNWs grown at 400 °C for two different SiH_4/H_2 feed-gas ratios and two different durations. The wires are cylindrical and randomly oriented relative to the substrate with a significant increase in the wire diameter and length as the growth duration is increased. In the images of the larger diameter wires (Figure 1(b) and (d)), a texturing or roughness of the surface is visible. High-resolution TEM images provide a clearer picture of the structure of the SiNW surface (Figure 2(a) and (b)), showing that the wires exhibit a crystalline core with a polycrystalline shell. The ratio of core diameter to shell thickness varies with growth condition and increases toward the seed end of the wire. The SiNW shown in Figure 2(a) has a crystalline core of ~10 nm diameter and polycrystalline shell that is ~60 nm thick. It also exhibits twin/stacking fault defects in the core which were observed in a number of the wires. The shell is smaller relative to the core in the image in Figure 2(b) taken near the seed end of a different wire. The polycrystalline nature of the shell is more apparent in Figure 2(a)

because more of the nanocrystallites in this wire's shell are crystallographically aligned with the core than for the wire in Figure 2(b). Both shells, however, are polycrystalline. In addition, the crystallites in the shell region in Figure 2(a) are more defective than those in Figure 2(b). Both wires came from the same sample, and these types of wire to wire variations were routinely observed.

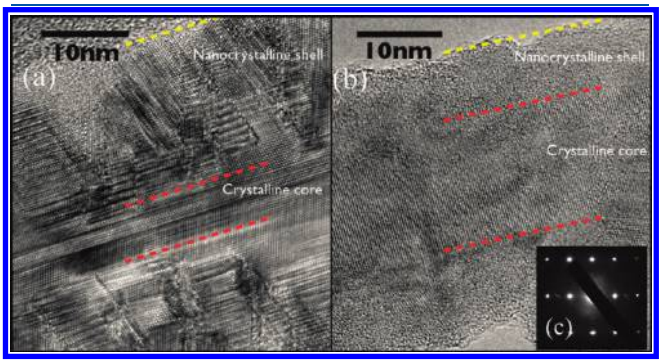

Figure 2. High-resolution TEM images of two Sn-seeded SiNWs showing crystalline cores ~10 nm (a) and ~20 nm (b) in diameter with nanocrystalline shells. A SAD pattern for the wire in (b) in which diffraction from the core dominates is shown in (c). These wires were grown for 8 min at 20 W of plasma power, with a flow of 100 sccm of H_2 (partial pressure of 1.35 Torr), 4 sccm of SiH_4 (partial pressure of 0.05 Torr) at 400 °C, and 1.4 Torr total chamber pressure.

In the selected area diffraction (SAD) pattern of the wire in Figure 2(b) which is shown in Figure 2(c), diffraction from the crystalline core dominates. The shell is formed because radial growth of the wire occurs in parallel with axial VLS growth of the core. This conclusion is supported by the decrease in shell size toward the seed end of the wires and tapering along the wire length discussed later. Raman scattering studies of the nanowires provide evidence that amorphous material is also present in the arrays. While this could arise from amorphous deposition on the substrate, we cannot rule out the possibility that it may indicate the shell is a mixture of crystalline and amorphous material analogous to nanocrystalline Si.[33]

Systematic studies were performed to understand the dependence of radial and axial growth rates on process variables. One way to effectively control the growth rates was through H_2 dilution of SiH_4, holding other process parameters constant. This is illustrated in Figures 3(a) and (b) which show the dependence of the average wire diameter and length on growth duration for the same two H_2 dilutions used in obtaining the wires in Figure 1. The average diameter was determined by measuring the diameter midway along the axial direction for a large number of wires. Determination of an average wire length was more complicated because of the scatter in length seen in Figure 1. As discussed below, this scatter probably arises from etching of the Sn during the growth process which causes wires with smaller diameter seeds to stop lengthening before the growth cycle is complete. Hence only the longest ~10% of the

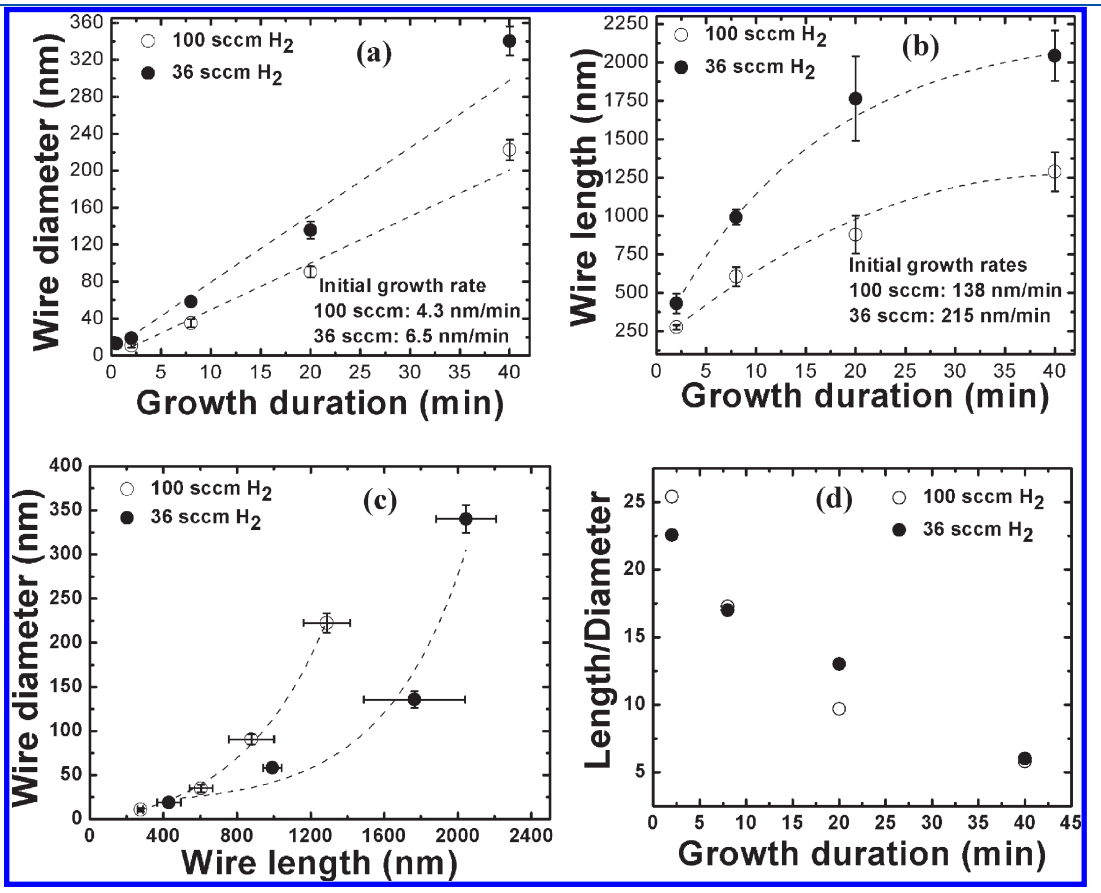

Figure 3. SiNWs (a) diameter and (b) length as a function of growth duration. (c) SiNW diameter as a function of length. (d) Aspect ratio of the wires plotted against growth duration. H_2 flow rates of 100 (1.35 Torr partial pressure) and 36 sccm (1.26 Torr partial pressure) correspond to H_2 to SiH_4 dilutions of 25:1 and 9:1, respectively.

dx.doi.org/10.1021/jp1066428 |J. Phys. Chem. C 2011, 115, 3833–3839

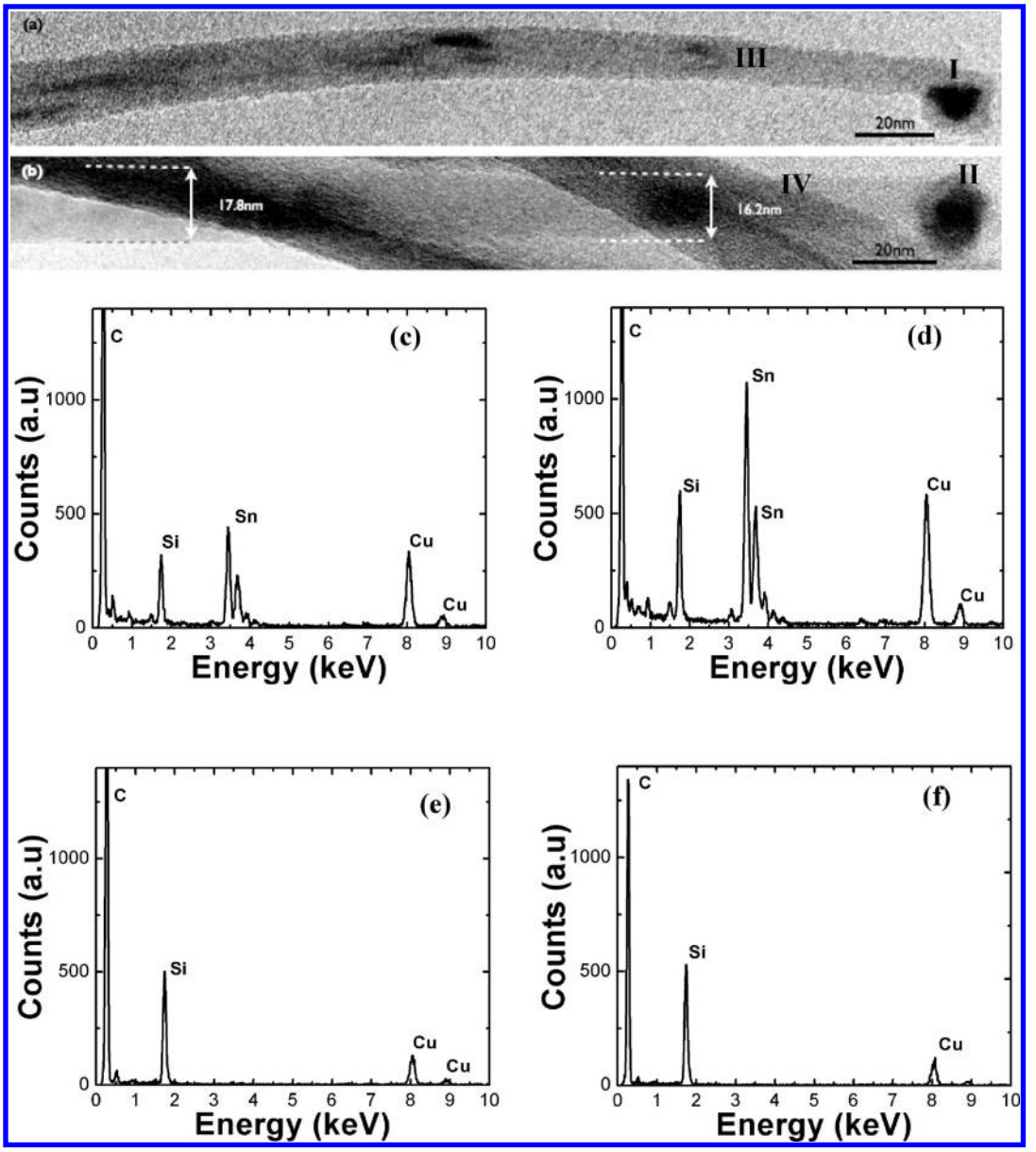

Figure 4. (a) and (b) are two nanowires grown for 2 min. (c)−(f) are XEDS spectra collected under TEM mode by focusing the electron beam at positions I−IV indicated in (a) and (b), respectively. The collection time was 2 min. A strong Sn signal is observed for both the SiNWs at the tip. The Cu peak is from the TEM grid, and the C peak is from the supporting carbon film.

wires were considered in determining the average length. While this definition is somewhat arbitrary, it is sufficient to illustrate several important aspects of the axial growth rate.

Figures 3 (a) and (b) show that the wires were both thicker and longer for lower H_2 dilution (36 sccm versus 100 sccm corresponding to 9:1 versus 25:1 H_2:SiH_4 flow ratio). The initial growth rates indicated in the figures are based on the data point at 2 min. Compared to VLS-based growth in the axial direction, the initial growth rate in the radial direction was slower by at least a factor of 30. The increase in SiNW diameter was approximately linear with time (Figure 3(a)), while the axial growth rate (Figure 3(b)) decreased as a function of time. Examination of Figure 3(c), which plots wire diameter versus length, reveals that wire length saturates at a value that depends on the H_2/SiH_4 ratio. The higher the H_2 dilution, the shorter the wire when axial growth terminates.

Saturation of wire length was caused by loss of the Sn seed as growth proceeds. Figure 4(a) and (b) show TEM images of nanowires grown for 2 min, which is much less than the time for axial growth to saturate. Sn seeds are clearly visible at the growth end of the wires as confirmed by the X-ray energy dispersive spectroscopy (XEDS) measurements on the wire tips shown in Figure 4(c) and (d). In addition, within the XEDS detectability limit, Sn is not observed at other locations such as shown in Figure 4 (e) and (f). Figure 5(a) is the TEM image of a wire grown for 20 min, at which point axial growth has stopped. There is no evidence of Sn in the XEDS measurement at the wire tip (Figure 5(b)) or at any other location on the wire (Figure 5(c), for example). There are several possible explanations for the disappearance of the Sn seed. For example, a reduction in size and eventual disappearance of the seed have previously been reported in VLS growth of Si nanowires and attributed to metal

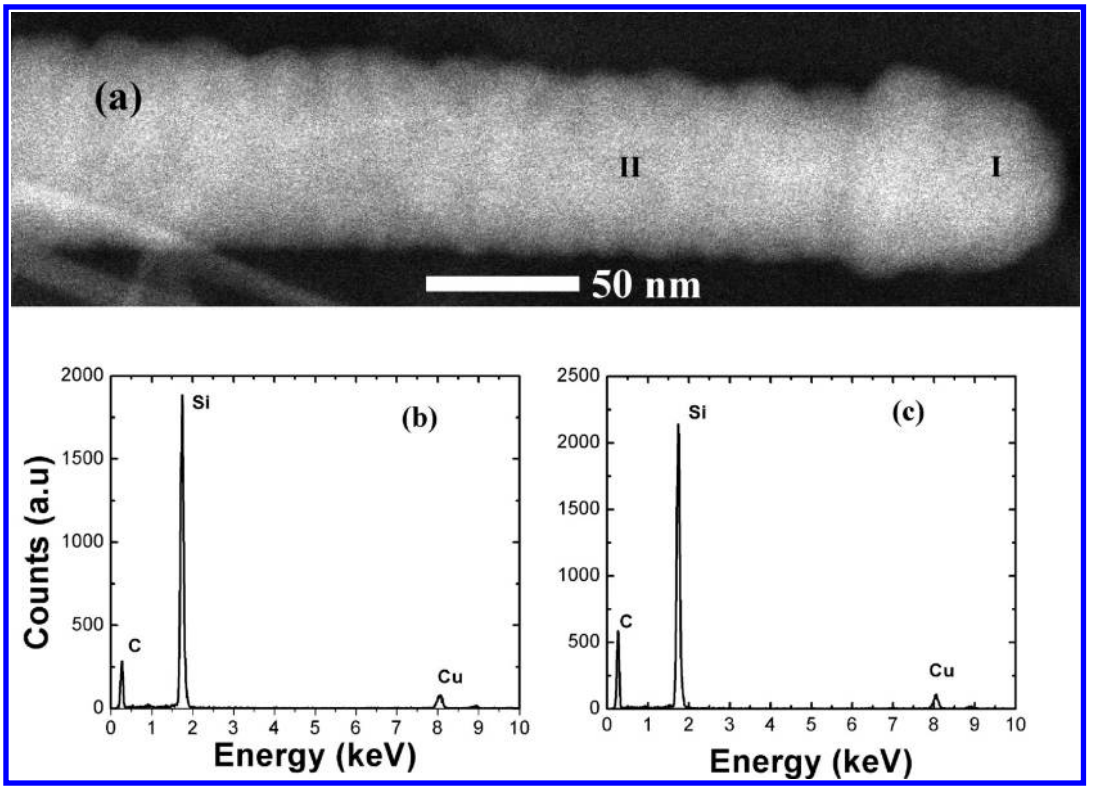

Figure 5. (a) Annular-dark-field STEM image near the tip of a nanowire grown for 20 min. (b) and (c) are XEDS spectra collected near region I (where the metal catalyst might be expected to be present) and II, respectively. A strong Si signal is observed for both the SiNW body and the tip. Sn, however, was below the detection limit of XEDS (<~1%). The Cu peak is from the TEM grid, and the C peak is from the supporting carbon film.

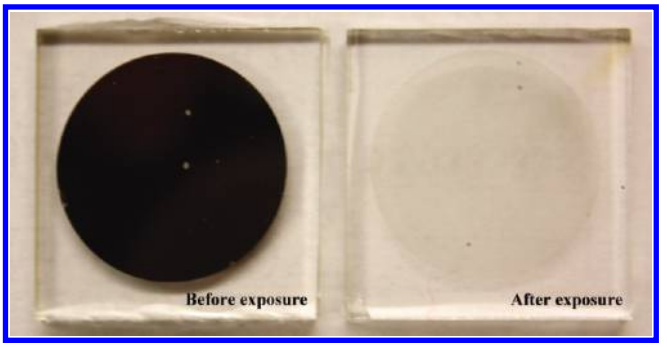

Figure 6. Optical images of (a) Sn (50 nm) coated glass prior to H_2 plasma exposure and (b) residual Sn on the surface of glass after a 20 min H_2 plasma treatment.

diffusion along the wire walls and/or dissolution of the seed metal in the silicon.[34] Within the detection limit of XEDS, we see no evidence of Sn on the wire sidewalls or on any other location including the substrate. At the growth temperature of 400 °C, Sn is practically insoluble in Si.[21] If Sn were present in the wire interior, it would probably be in the form of metal inclusions. However, none of our TEM or XEDS measurements showed any indication of Sn inclusions. Sn could be present at levels below the XEDS detection limit. We believe, however, the more likely explanation is that the Sn is removed from the wire tip through etching by atomic H generated in the plasma which results in formation of volatile tin hydrides (e.g., SnH_4 or Sn_2H_6). Other group IV elements such as C, Si, and Ge are also known to etch in the presence of atomic H, and there are prior reports of using atomic H to etch Sn.[35−39] To support this explanation, Figure 6 shows images before and after H_2 plasma treatment of a 50-nm-thick Sn layer on glass that was exposed to an H_2 plasma at a pressure comparable to H_2 partial pressures used during nanowire growth. The Sn layer decreased in thickness at an etch rate of ~0.5 nm/min. This is consistent with the observation that VLS growth attenuated after about 20 min assuming an initial seed diameter of ~20 nm which is a typical core diameter. Given the removal of the Sn seeds, the nature of the seedlike feature at the tip of wires grown for 20 min in Figures 1(b) and (d) and 5 (a) is interesting. These features are clearly much larger than the actual seeds (visible in Figures 1(a) and (c) and 4(a) and (b)) that lead to the crystalline cores. We speculate they arise from enhanced vapor−solid (VS) growth (discussed next) at the end of the wire after axial growth has terminated; however, the exact nature of the feature is an open question. Also of interest is the obvious tapering in the wires grown for 2 min shown in Figure 4(a) and (b), which is consistent with core shell growth. Such tapering is also observed in longer growths as mentioned above. It is, however, less obvious because radial growth continues after axial growth stops, resulting in wires which are thick relative to the length. Once the wires have significantly grown in the radial direction, the difference in diameter between the base and tip becomes a small fraction of the average diameter, and the nanowires appear to be more cylindrical.

Radial growth of group IV nanowires prepared by thermal CVD has been discussed in terms of uncatalyzed VS growth.[40] In contrast, Li et al.[41] argued rough side wall formation on Au seeded Ge wires can arise from a vapor−solid−solid (VSS) type of radial growth resulting from catalyst migration onto the side wall of the wires. In the present case, the much lower radial growth rate, absence of elemental Sn on the walls, and constant

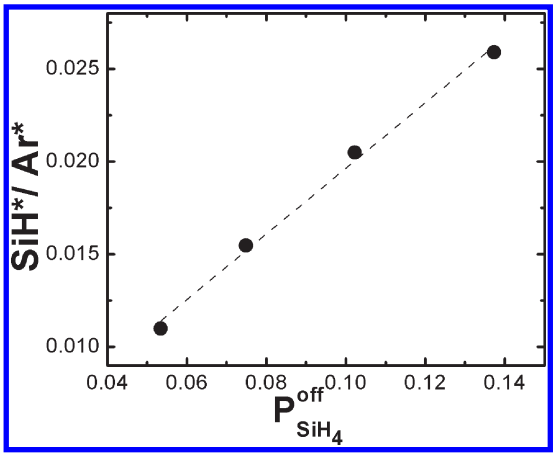

Figure 7. Ratio of the SiH* to Ar* emission intensities as a function of the SiH_4 partial pressure in the feed gas ($P_{SiH_4}^{off}$). (For details, see Supporting Information.)

rate of radial growth even after the Sn seeds have been etched away argue against this mechanism. It seems likely a direct VS growth mechanism is primarily responsible for the shell growth observed here. It is interesting to note that multiplying both the wire diameter and the wire length curves for 100 sccm H_2 growth in Figure 3(a) and (b) by 1.5 causes them to virtually overlay curves for 36 sccm H_2 growth. This is evident in the plots of aspect ratio (length to diameter ratio) as a function of the growth duration in Figure 3(d) which are virtually the same for both H_2 dilution conditions.

To better understand how changes in H_2 dilution affect radial and axial growth rates, optical emission spectroscopy (OES) measurements were made of the plasma using Ar as an actinometer (Figure 7).[42] This technique has been extensively employed to probe SiH_4/H_2 plasmas.[32,42−44] The SiH_4 partial pressure was varied by changing the H_2 flow rate between the 36 and 100 sccm values used in the growth rate measurements in Figure 3. Figure 7 shows that the normalized SiH* emission intensity increases linearly with SiH_4 partial pressure in the feed gas. The SiH* density in our reactor is proportional to the partial pressure of the SiH_x ($x = 0−3$) radicals in the plasma, which are primarily responsible for growth (for details see Supporting Information and ref 45). This implies that as the H_2 content of the plasma increases the concentration of dissociated SiH_4 decreases and the growth rate drops. An alternative explanation for reduced growth rate with higher hydrogen dilution involves Si deposition occurring simultaneously with atomic H-induced etching of the silicon surface. Reduced amorphous silicon growth rates with increased hydrogen dilution have been attributed to this effect.[46] However, when SiNWs were exposed to an H_2 plasma for different durations immediately after growth, no noticeable change in the wire diameter or length was observed. This is consistent with the reported etch rates of crystalline Si by atomic H, which are very low at the growth temperature of ~400 °C.[47] This leads to the conclusion that the primary influence of hydrogen dilution on growth rate is through its effect on SiH_4 dissociation.

4. CONCLUSIONS

In summary, PECVD growth of Sn-seeded SiNWs has been demonstrated over temperatures from 300 to 400 °C which are compatible with low-cost glass substrates and a number of flexible plastic substrate materials. The wires exhibited a crystalline core arising from axial VLS growth and a polycrystalline shell due to radial VS deposition. Growth rate control was demonstrated through H_2 dilution which affects the concentration of the reactive SiH_x radicals involved in growth. The relative rate of radial to axial growth was, however, essentially independent of H_2 partial pressure for the range of conditions explored. Particularly intriguing from a device perspective is the consumption of the Sn seed by the H_2 plasma. While this creates an additional variable to control, it also opens up the possibility of self-limiting growth at a fixed length from mono size-dispersed Sn seeds and of producing metal-free nanowire arrays for device applications without a separate metal etch step.

■ ASSOCIATED CONTENT

Supporting Information. Additional experimental details. This material is available free of charge via the Internet at http://pubs.acs.org.

■ AUTHOR INFORMATION

Corresponding Author
*E-mail: rtcollin@mines.edu.

■ ACKNOWLEDGMENT

This material is based upon work supported by the National Science Foundation through the Renewable Energy Materials Research Science and Engineering Center under Grant No. DMR-0820518, the Center for Revolutionary Solar Photoconversion, and DOE under contract No. DE- PS36-07GO94025. This support is gratefully acknowledged. The authors thank Dr. John Chandler for his assistance with SEM measurements.

■ REFERENCES

(1) Wagner, R. S.; Ellis, W. C. *Appl. Phys. Lett.* **1964**, *4*, 89.
(2) Read, A. J.; Needs, R. J.; Nash, K. J.; Canham, L. T.; Calcott, P. D. J.; Qteish, A. *Phys. Rev. Lett.* **1992**, *69*, 1232.
(3) Cui, Y.; Lauhon, L. J.; Gudiksen, M. S.; Wang, J.; Lieber, C. M. *Appl. Phys. Lett.* **2001**, *78*, 2214.
(4) Garnett, E.; Yang, P. *Nano Lett.* **2010**, *10*, 1082.
(5) Kelzenberg, M. D.; Boettcher, S. W.; Petykiewicz, J. A.; Turner-Evans, D. B.; Putnam, M. C.; Warren, E. L.; Spurgeon, J. M.; Briggs, R. M.; Lewis, N. S.; Atwater, H. A. *Nat. Mater.* **2010**, *9*, 239.
(6) Cui, Y.; Zhong, Z.; Wang, D.; Wang, W. U.; Lieber, C. M. *Nano Lett.* **2003**, *3*, 149.
(7) Schmidt, V.; Riel, H.; Senz, S.; Karg, S.; Riess, W.; Gosele, U. *Small* **2006**, *2*, 85.
(8) Stelzner, T.; Pietsch, M.; Andra, G.; Falk, F.; Ose, E.; Christiansen, S. *Nanotechnology* **2008**, *19*, 295203.
(9) Yu, D. P.; Bai, Z. G.; Ding, Y.; Hang, Q. L.; Zhang, H. Z.; Wang, J. J.; Zou, Y. H.; Qian, W.; Xiong, G. C.; Zhou, H. T; Feng, S. Q. *Appl. Phys. Lett.* **1998**, *72*, 3458.
(10) Holmes, J. D.; Johnston, K. P.; Doty, R. C.; Korgel, B. A. *Science* **2000**, *287*, 1471.
(11) Liu, J. L.; Cai, S. J.; Jin, G. L.; Tang, Y. S.; Wang, K. L. *Superlattices Microstruct.* **1999**, *25*, 477.
(12) Yang, W.-C.; Zeman, M.; Ade, H.; Nemanich, R. J. *Phys. Rev. Lett.* **2003**, *90*, 136102.
(13) Yu, J.-Y.; Chung, S.-W.; Heath, J. R. *J. Phys. Chem. B* **2000**, *104*, 11864.
(14) Schmidt, V.; Wittemann, J. V.; Senz, S.; Gösele, U. *Adv. Mater.* **2007**, *21*, 2681.
(15) Sze, S. M. *Physics of Semiconductor Devices*; Wiley: New York, 1981; Vol. 1.

(16) Kamins, T. *Semiconductor nanowires for electronics and sensors*, HE-Heraeus-Seminar; Semiconductiong Nanowires: Physics, Materials and Devices, 2007; Vol. *397*.
(17) Li, N.; Tan, T. Y.; Gosele, U. *Appl. Phys. A: Mater. Sci. Process.* **2008**, *90*, 591–596.
(18) Fanciulli, M.; Byberg, J. R. *Phys. B* **1999**, *273*, 524.
(19) Li, C. P.; Wang, N.; Wong, S. P.; Lee, C. S.; Lee, S.-T. *Adv. Mater.* **2002**, *14*, 218.
(20) Baron, T.; Gordon, M.; Dhalluin, F.; Ternon, C.; Ferret, P.; Gentile, P. *Appl. Phys. Lett.* **2006**, *89*, 233111.
(21) Olesinski, R. W.; Abbaschian, G. J. *Bull. Alloy Phase Diagrams* **1984**, *5*, 273.
(22) *American Institute of Physics Handbook*, 3rd ed.; McGraw-Hill: New York, 1972; pp 4−243.
(23) Hofmann, S.; Ducati, C.; Neill, R. J.; Piscanec, S.; Ferrari, A. C.; Geng, J.; Dunin-Borkowski, R. E.; Robertson, J. *J. Appl. Phys.* **2003**, *94*, 6005.
(24) Sharma, S.; Sunkara, M. K. *Nanotechnology* **2004**, *15*, 130.
(25) Aella, P; Ingole, S.; Petuskey, W. T.; Picraux, S. T. *Adv. Mater.* **2007**, *19*, 2603.
(26) Iacopi, F.; Vereecken, P. M.; Schaekers, M.; Caymax, M.; Moelans, N.; Banpain, B.; Richard, O.; Detavernier, C.; Griffiths, H. *Nanotechnology* **2007**, *18*, 505307.
(27) Chi, H.; Zhu, H.-C.; Xu, H.-J.; Shan, X.-D.; Liao, Z.-M.; Yu, D.-P. *J. Phys. Chem. C* **2009**, *113*, 6450.
(28) Yu, L.; O'Donnell, B.; Alet, P.-J.; Conesa-Boj, S.; Peiró, F.; Arbiol, J.; Cabarrocas, P. R. i. *Nanotechnology* **2009**, *20*, 225604.
(29) Yu, L.; O'Donnell, B.; Maurice, J.-L.; Cabarrocas, P. R. i. *Appl. Phys. Lett.* **2010**, *97*, 023107.
(30) Jeon, M.; Uchiyama, H.; Kamisako, K. *Mater. Lett.* **2009**, *63*, 246.
(31) Parlevliet, D.; Cornish, J. C. L. *Mater. Res. Soc. Symp. Proc.* **2007**, *989*, 0989–A23−03.
(32) Kampas, F. J.; Griffith, R. W. *J. Appl. Phys.* **1981**, *52*, 1285.
(33) Matsuda, A. *J. Non-Cryst. Solids* **1983**, *59*−*60*, 767–774.
(34) Hanon, J. B.; Kodambaka, S.; Ross, F. M.; Tromp, R. M. *Nature* **2006**, *440*, 69.
(35) Muranaka, Y.; Yamashita, H.; Miyadera, H. *Thin Solid Films* **1991**, *195*, 257–272.
(36) Zheng, Y.-J.; Ma, P. F.; Engstrom, J. R. *J. Appl. Phys.* **2001**, *90*, 3614.
(37) Abrefah, J.; Olander, D. R. *Surf. Sci.* **1989**, *209*, 291.
(38) Pearsson, T. G.; Robinson, P. L.; Stoddart, E. M. *Proc. R. Soc. London A* **1933**, *142*, 275.
(39) Van Herpen, M. M. J. W.; Klunder, D. J. W.; Soer, W. A.; Moors, R.; Banine, V. *Chem. Phys. Lett.* **2010**, *484*, 197.
(40) Lauhon, L. J.; Gudiksen, M. S.; Lieber, C. M. *Philos. Trans. R. Soc. London, Ser. A* **2004**, *362*, 1247.
(41) Li, C. B.; Usami, K.; Mizuta, H.; Oda, S. *J. Appl. Phys.* **2009**, *106*, 046102.
(42) Kampas, F. J. *J. Appl. Phys.* **1983**, *54*, 2276.
(43) van den Donker, M. N.; Rech, B.; Finger, F.; Kessels, W. M. M.; van de Sanden, M. C. M. *Appl. Phys. Lett.* **2005**, *87*, 263503.
(44) Dingemans, G.; van den Donker, M. N.; Hrunski, D.; Gordijn, A.; Kessels, W. M. M.; van de Sanden, M. C. M. *Appl. Phys. Lett.* **2008**, *93*, 111914.
(45) Howling, A. A.; Strahm, B.; Hollenstein, C. *Thin Solid Films* **2009**, *517*, 6218.
(46) Tsai, C. C.; Anderson, G. B.; Thompson, R.; Wacker, B. *J. Non-Cryst. Solids* **1989**, *114*, 151.
(47) Veprek, S.; Sarott, F.-A. *Plasma Chem. Plasma Process.* **1982**, *2*, 3.